





Improvements in the Compression Filter and Calibration Factor of the Progressive Pulse Compression Technique

Cesar M. Salazar , *Member, IEEE*, Boonleng Cheong , Robert D. Palmer , *Fellow, IEEE*,
David Schwartzman , *Senior Member, IEEE*, Alexander Ryzhkov

Abstract—Progressive Pulse Compression (PPC) was introduced to mitigate the need for a fill pulse in pulse-compression-based radar systems. It provides a method for recovering signals in the blind-range region created by the transmission of relatively long pulses. However, the initial implementation of PPC has limitations that need to be addressed for it to be more useful for meteorological applications. The proposed updated algorithm, named herein PPC+, brings significant improvements to mitigate these limitations. The methodology of PPC+ is similar to that of PPC, except that it uses a set of improved pulse compression filters. The improved compression filters are designed based on an amplitude modulation approach and are generated by multiplying the original filter by a range-dependent window. The window can be divided into two sections, the first part has a number of nulled samples used for mitigating the mainlobe migration, and the remaining portion is a number of tapered samples to alleviate the “shoulder” effect from range sidelobes. Also, in contrast to PPC, the calibration factor used in PPC+ is further tuned to account for the tapering used in the improved compression filters. The PPC+ technique has been tested using data collected with PX-1000, a polarimetric X-band transportable solid-state radar system designed and operated by the Advanced Radar Research Center (ARRC) at the University of Oklahoma, and it is implemented and operational on that system (data available at <https://radarhub.rrc.ou.edu>). This technique has also been implemented on Horus, a fully digital phased array radar recently completed at the ARRC.

Index Terms—Pulse compression, signal processing, weather radar, solid-state amplifier, bandwidth.

I. INTRODUCTION

C. M. Salazar is with Advanced Radar Research Center and the Cooperative Institute for Severe and High-Impact Weather Research and Operations at The University of Oklahoma, Norman, OK 73019 USA.

B. Cheong is with the Advanced Radar Research Center at The University of Oklahoma, Norman, OK 73019 USA.

R. D. Palmer and D. Schwartzman are with the Advanced Radar Research Center and the School of Meteorology at The University of Oklahoma, Norman, OK 73019 USA.

A. Ryzhkov is with the Cooperative Institute for Severe and High-Impact Weather Research and Operations, the School of Meteorology, and the Advanced Radar Research Center at The University of Oklahoma, Norman, OK 73019 USA.

Funding was provided by NOAA/Office of Oceanic and Atmospheric Research under NOAA-University of Oklahoma Cooperative Agreement #NA21OAR4320204, U.S. Department of Commerce. The authors would like to thank the ARRC leadership and the ARRC engineers for their support and design/research/development efforts.

Manuscript received August XX, 2023; revised XX YY, 2023.

THE blind range is an inherent artifact on systems that use pulse compression [1–8], e.g., solid-state dish-based radars and modern phased array radars. The blind range is a by-product of transmitting a long modulated pulse necessary for increasing system sensitivity when using relatively low-powered solid-state amplifiers [7, 9, 10]. When a radar is transmitting, it does not usually receive useful information. This is because the transmitted waveform leaks into the receiver, contaminating a portion of the received signal and causing the so-called blind range. The blind range, denoted as R_b , in units of m, is directly proportional to the pulse width of the transmitted pulse τ , in units of s, as described by Salazar *et al.* [8] and Salazar [11] (see Equation (1) extracted from Salazar [11]),

$$R_b = R_p = \frac{c\tau}{2}, \quad (1)$$

where c is the speed of light, in m s^{-1} , and R_p is the pulse length in m.

Different techniques to mitigate the blind range have been discussed in the literature. One widely used strategy is to use a “fill pulse” to recover the data inside the blind range [e.g. 3–5]. However, the fill pulse is much shorter than the long pulse, resulting in significantly lower sensitivity inside the blind range. In addition, this method requires additional bandwidth since the fill pulse is transmitted at a separate carrier frequency. Alternatively, the blind range can be mitigated using a bistatic radar system (hardware-based solution), where the transmitter and receiver chains are independent [12–14]. This increases the cost and complexity of weather radar systems, compared to the more traditional monostatic radars. Adopting a bistatic radar approach would require additional hardware (i.e., cost) and synchronizing the transmitter/receiver to get coherent measurements useful for Doppler moment estimation (a typical challenge with bistatic systems). Lastly, different novel signal processing solutions to mitigate the blind range using the uncontaminated portion of the received signal from the long pulse have been proposed [e.g. 8, 11, 15, 16]. One of those techniques is the progressive pulse compression (PPC) technique, proposed by Salazar *et al.* [8].

PPC is simple to implement since it requires no hardware modification. Moreover, its implementation is potentially less expensive when compared to the techniques using fill pulses since it does not require the extra bandwidth necessary to accommodate those pulses. More importantly, the sensitivity

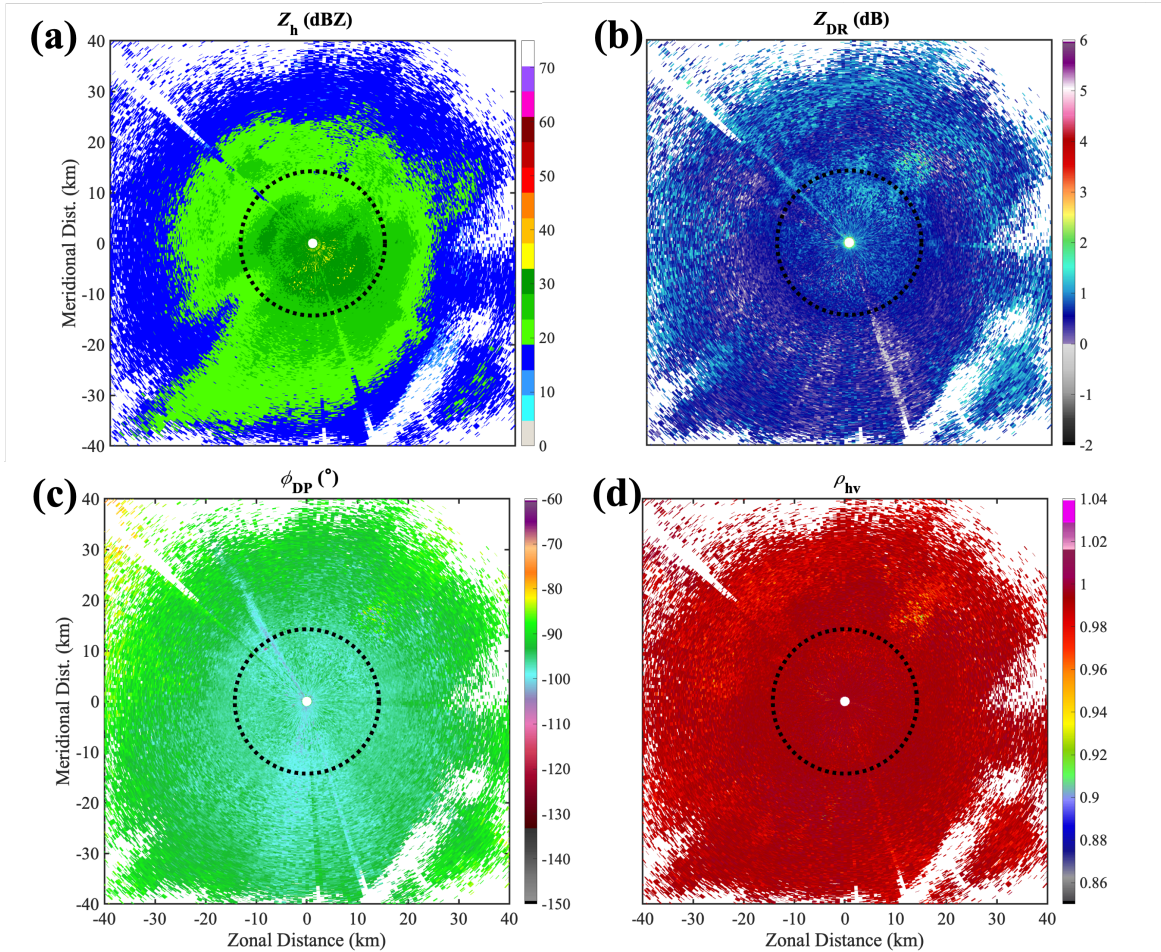


Fig. 1. PPIs of different radar variables processed using PPC, at an elevation angle of 4° : a) radar reflectivity factor from the horizontal channel (Z_h), b) differential reflectivity (Z_{DR}), c) differential phase (ϕ_{DP}), and d) correlation coefficient (ρ_{hv}), from a snow event observed in the Oklahoma City metropolitan area on February 3, 2022, 01:57 UTC.

inside the blind range is higher when compared to techniques using fill pulses, and it has a seamless transition in sensitivity from the blind to the visible range. Therefore, when successful, the PPC technique can more effectively mitigate the blind range [8, 11]. Nevertheless, even though the sensitivity is higher than that provided by a fill pulse, there is a gradual loss in sensitivity proportional to the range to the radar (see the Sensitivity Analysis section in Salazar *et al.* [8]).

PPC was implemented on the PX-1000 system, an X-band transportable solid-state polarimetric radar designed and operated by the Advanced Radar Research Center (ARRC) at The University of Oklahoma (OU) [5]. It has been operational on PX-1000 since 2020, and has been used in different field campaigns to collect meteorological data from various events (e.g., supercell storms, squall-line storms, and snowstorms). One such dataset was a snow event in the metropolitan area of Oklahoma City on February 3, 2022. Raw IQ data from that event were collected and compressed using PPC. Polarimetric variables derived from the IQ data of a plane-position indicator (PPI) scan at 01:57 UTC, and at an elevation angle of 4° are shown in Fig. 1. The variables include radar reflectivity factor (Z_h), differential reflectivity (Z_{DR}), differential phase (ϕ_{DP}),

and correlation coefficient (ρ_{hv}).

The blind range corresponding to the data shown in Fig. 1 (delineated by black dashed circles) is approximately 14.2 km ($\tau = 95 \mu\text{s}$). As apparent in Fig. 1, there is no obvious difference between the “blind” range and the visible range in any of the polarimetric variables illustrated. This seamless transition is generated by the sensitivity increase inside the “blind” range compared to other implementations using fill pulses. Therefore, it can be said that the blind range is mostly mitigated. Nonetheless, in immediate vicinity of the radar (less than 1 km away in range), different factors, such as the radiation properties in the antenna near-field region or the incorrect estimation of scatterers due to the minimal amount of uncontaminated IQ data, produce a small blind range that cannot be mitigated by PPC. This region is termed the inherent blind range. To avoid confusion, the old blind range, including both the inherent and mitigated blind ranges, will be referred to as the transmission range. Nevertheless, since the inherent blind range cannot be mitigated, it will not be considered when evaluating the performance of the techniques discussed in this work.

The PX-1000 system is constantly upgraded through soft-

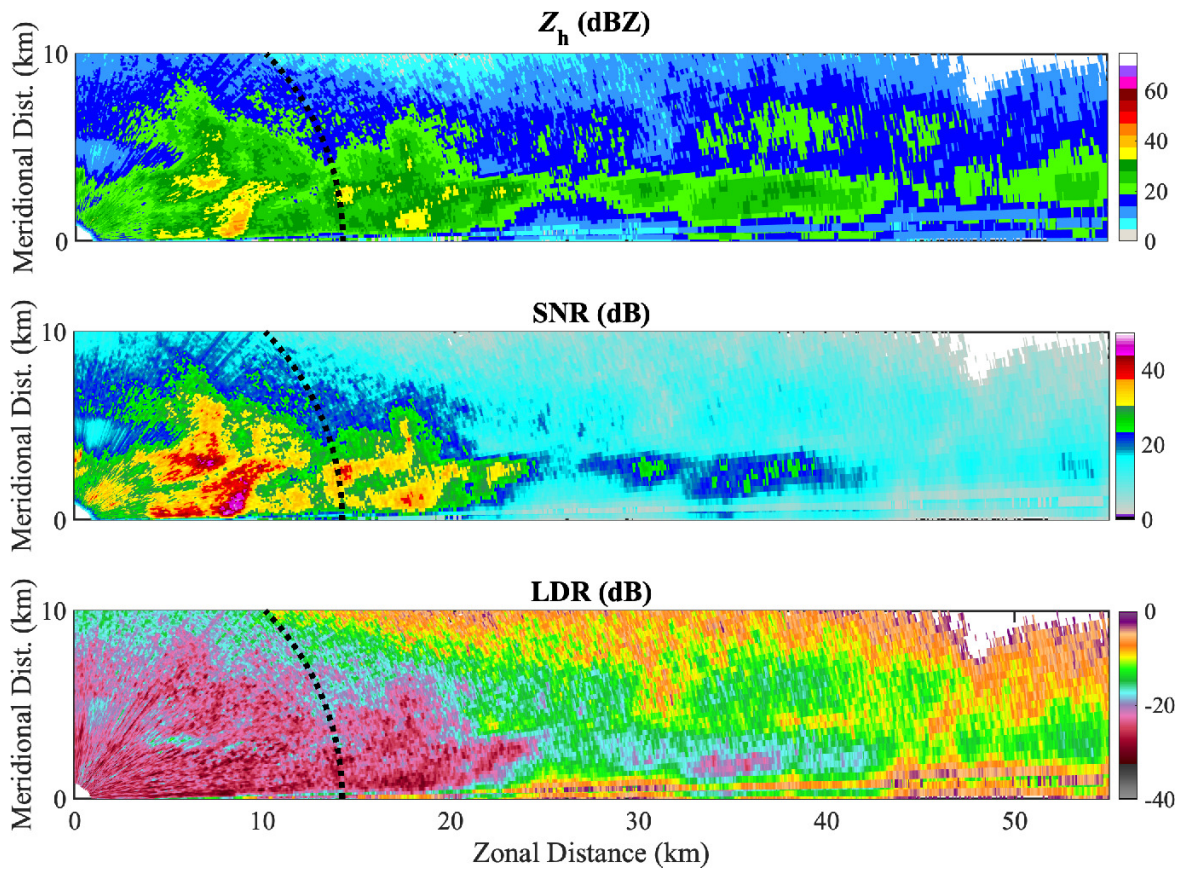


Fig. 2. RHI plots of different radar variables processed using PPC: Z_h (top plot), SNR (middle plot), and LDR (bottom plot), from a storm event observed with the ATSR mode on May 23, 2022, 16:33 UTC.

ware modifications, and different transmission modes are being tested for future meteorological studies. One example is the alternate transmission simultaneous reception (ATSR) mode of H/V polarizations [17], where PPC has proven applicable. In Fig. 2, three polarimetric variables calculated from raw IQ data collected in the ATSR mode and compressed using PPC are presented. The variables are the radar reflectivity factor from the horizontal channel (Z_h) (top panel), signal-to-noise ratio (SNR) (middle panel), and linear depolarization ratio (LDR) (bottom panel). The data were extracted from a range-height indicator (RHI) scan collected during a convective thunderstorm event on May 23, 2022, 16:33 UTC.

This seamless transition across the transmission range is important in generating radar variables that are derived from close-range data, such as the quasi-vertical profiles (QVP) [18]. QVPs consist of an inventive way to emulate the results from vertical profilers using PPI scans collected at high elevations [18]. Fig. 3 illustrates the QVPs of Z_h (left plot), Z_{DR} (center plot), and ρ_{hv} (right plot) generated from a snow event in the Oklahoma City metropolitan area on February 3, 2022, 02:37 UTC (PPI scan at 12° elevation). Data were collected with the PX-1000 radar and the polarimetric variables were derived from raw IQ data compressed using PPC.

The equivalent transmission ranges shown in Fig. 3 can be calculated from the PPI elevation angle and the pulse width ($\tau = 95 \mu\text{s}$). In this case, approximately the first 3 km in

height correspond to the transmission range (delimited with red lines). Similar to previous experiments, when using PPC for compression, there is a smooth transition in the values of Z_h , Z_{DR} , and ρ_{hv} across the transmission range.

Even with all these advantages, PPC has some limitations that can be improved. Some have been discussed in Salazar *et al.* [8] and Salazar [11], mainly related to the so-called “shoulder” effect and the shift in the mainlobe peak position. These are by-products of the cross-correlation between the compression filter and the uncontaminated tail portion. After compression, the ambiguity (or range-weighting) function at zero Doppler of the point targets affected by this effect is asymmetrical, with large sidelobes especially prominent on one side (away from the radar) and a shifted mainlobe peak. Additionally, those larger sidelobes can be observed to be merged in the mainlobe and resemble shoulders, hence the name of this artifact. The shoulder effect is illustrated in Fig. 4, extracted from Salazar *et al.* [8] and Salazar [11]. These results were derived using a $67 \mu\text{s}$, 2.2-MHz non-linear frequency modulated (NLFM) waveform.

The shoulder effect can be significant in certain weather events with strong reflectivity gradients. This limitation is noticeable in the PPI plots presented in Fig. 5. These are polarimetric variables from a convective storm event on March 18, 2022, 00:33 UTC at an elevation angle of 2° and compressed using PPC.

In Fig. 5, contamination from the shoulders (smeared ra-

Quasi-Vertical Profiles

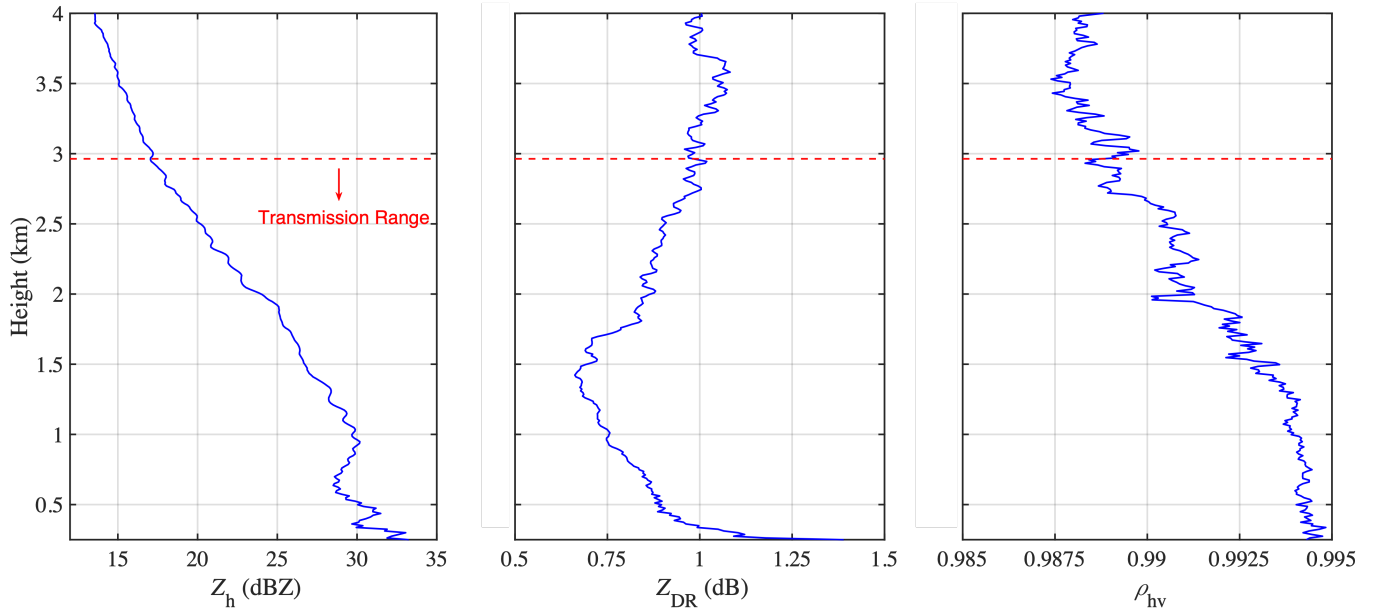


Fig. 3. QVP of Z_h (left plot), Z_{DR} (center plot), and ρ_{hv} (right plot) generated from a PPI collected during a snow event in the Oklahoma City metropolitan area on February 3, 2022, 02:37 UTC (12° in elevation).

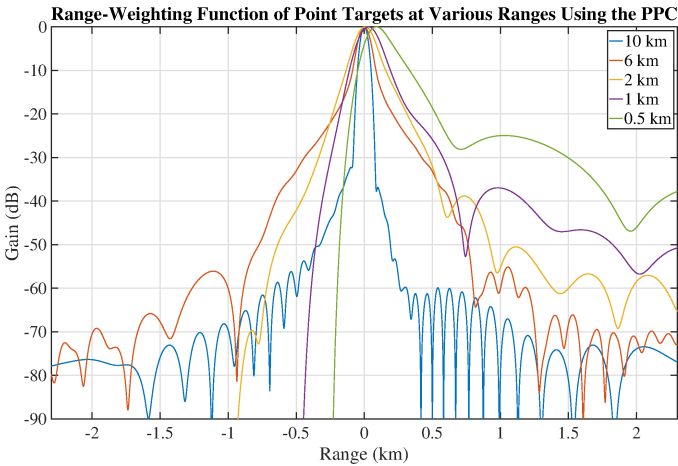


Fig. 4. Waveform range-weighting function of point targets at various ranges using a 2.2-MHz NLFM waveform. The figure has been sourced from Salazar *et al.* [8] and Salazar [11] and slightly edited for this work.

dials) can be observed to the northeast, southeast, and west regions of the transmission range (especially in the Z_h plot). The shoulders introduce biases and can obscure weaker echoes located in the same azimuth direction, shadowing the returns along the range. They contaminate both sides of the scatterers in the range direction. Moreover, this shadow becomes longer as the weather returns are closer to the radar.

This article presents an improved version of PPC, termed PPC+. The PPC+ technique presents a pivotal update required by the PPC users to make this technique more valuable for polarimetric weather observations. Similar to PPC, PPC+ is a signal-processing solution to mitigate the blind range without needing a fill pulse (nevertheless, there is still an inherent blind

range as explained previously). It improves over PPC mainly by replacing the compression filter used for partial decoding with a set of range-dependent improved compression filters (for weighted partial decoding). The improved compression filters use a smooth amplitude tapering function designed to mitigate the shoulder effect and the mainlobe migration.

PPC+ also includes a new calibration factor to preserve signal power in the range-dependent compression filters used. Weather radars aim not only to detect hydrometeors but also to quantify their polarimetric properties from compressed IQ data. However, PPC+ alters the compressed IQ data. Correctly calibrating the compressed IQ data in PPC+ allows the accurate estimation of the polarimetric measurements from scatterers within the transmission range. The derivation of this new calibration factor is presented in this article. The design of the improved compression filters has been analyzed to quantify the effects of the new taper function on the range resolution and radar sensitivity.

Compared to PPC, PPC+ can produce higher-quality polarimetric weather observations inside the transmission range without excessive sensitivity or range resolution degradation. The PPC+ technique is fully compatible with all transmission modes tested on PPC, including but not limited to PPIs, RHIs, and QVPs in both ATSR and its counterpart, the more commonly used simultaneous transmission simultaneous reception (STSR) mode of waves in the H/V polarizations. Moreover, by being an evolution of PPC, it can also be implemented as a software update on any radar system using pulse compression. Indeed, there are real-time operational implementations of PPC+ on radar systems, e.g., PX-1000. Real-time and archived polarimetric variable fields processed with PPC+ are available through the RadarHub (<https://radarhub.arcc.ou.edu>),

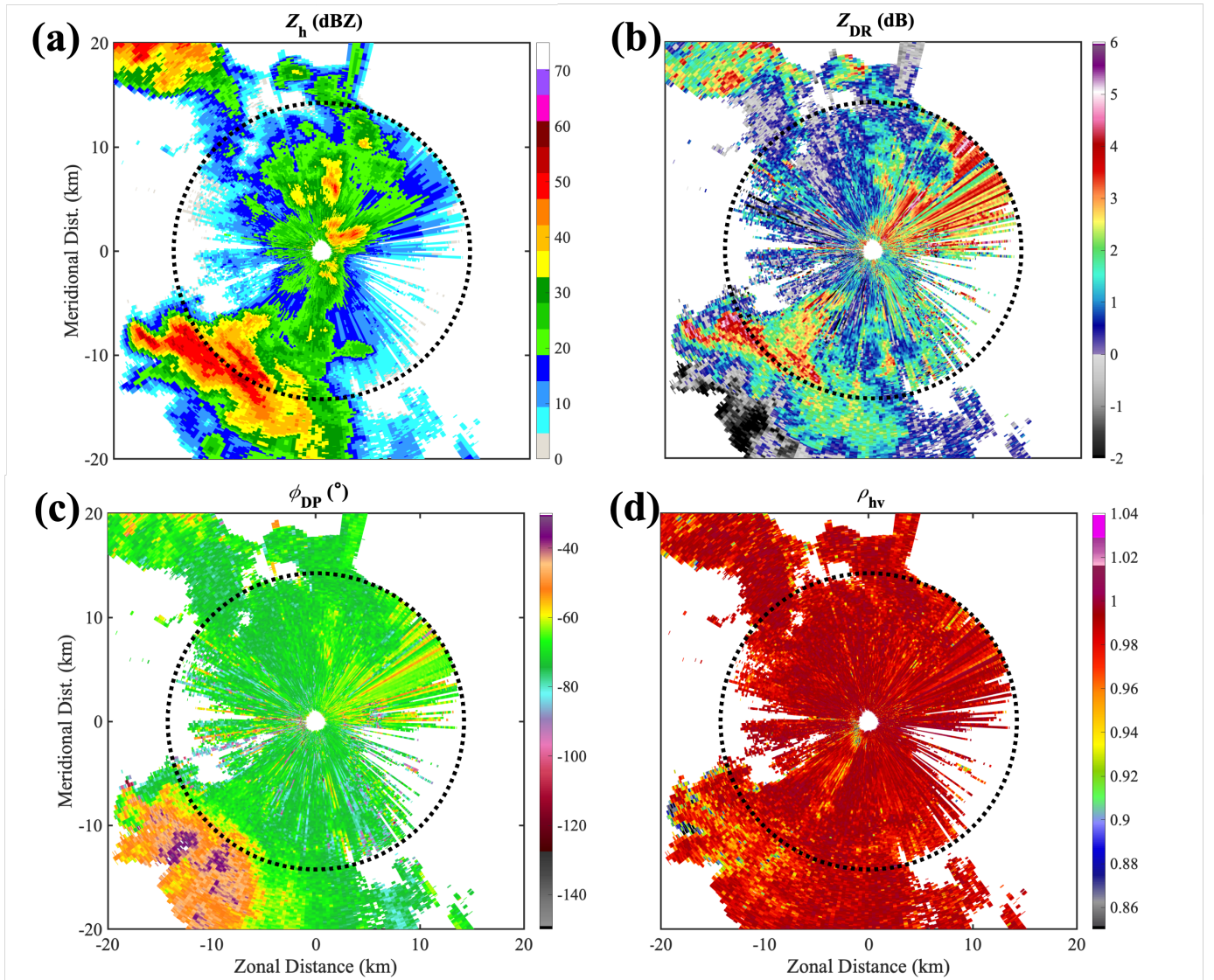


Fig. 5. PPI plots of different variables processed using PPC: a) Z_h (top plot), b) Z_{DR} , c) ϕ_{DP} , and d) ρ_{hv} , from a convective storm event observed on March 18, 2022, 00:33 UTC at an elevation angle of 2° .

since July 2023. The PPC+ technique has also been implemented in the Horus system, a state-of-the-art fully digital phased array radar recently completed at the ARRC [19–21].

The article is structured in three additional sections. Section II describes the improved PPC+ methodology, compared to the original PPC. This section also discusses the advantages and limitations of PPC+. Section III evaluates the improvements of PPC+ against the original PPC from simulated and actual weather data collected using the PX-1000 radar system. Finally, the discussion, conclusions, and future work are presented in Section IV.

II. PPC+ METHODOLOGY

As explained in the previous section, PPC+ consists of an improved version of PPC to mitigate some limitations observed in the original implementation. There are two main differences between PPC and PPC+. The first difference is the compression filter used. The PPC+ technique uses a set

of improved range-dependent compression filters. The second difference is the enhanced calibration factor derived for PPC+. The derivation of the improved compression filters and the calibration factor are detailed in the following section.

A. Improved Compression Filter Design and Partial Decoding

The improved compression filters are a modulated range-dependent version of the original compression filters. The improved compression filters replace the compression filter in the transmission range. There are three alternatives for the design of the improved compression filters, i.e., amplitude modulation, phase modulation, or a combination of amplitude and phase modulation [22]. This article considers a design based on amplitude modulation.

The design of each improved compression filter follows the same rules and can be conceptualized as a two-step process. Each step is designed to mitigate a specific limitation of PPC. In PPC, the received signal is multiplied by a window to

mitigate the contamination resulting in the blind range [8, 11, 23]. Nevertheless, as explained in the introduction, this modification also caused the mainlobe peak migration. Upon a detailed investigation of this effect, it was revealed that zeroing out some samples on each compression filter to match the number and location of the zeroes in the corresponding zeroed-out received signal at a specific range could significantly reduce migration of the mainlobe peak. The zeroing out is the first step in designing the improved compression filters, with the number of zeroes on each filter varying as a function of range.

Specifically, the number of zeroes on a particular improved compression filter can be estimated based on the principles illustrated in Fig. 6. From Fig. 6, the received signal has a target return located at R_t km (t_t μ s) that extends R_p km (τ μ s) further and ends at $(R_t + R_p)$ km ($t_t + \tau$ μ s). Additionally, the first R_b km (τ μ s) samples of the received signal are zeroed out due to contamination from the transmission. Therefore, the samples corresponding to the first $(R_b - R_t)$ km ($\tau - t_t$ μ s) of the target are zeroed out. Then, the improved compression filter to compress the signal at the range where the target is located should have the same number of samples zeroed out at the beginning.

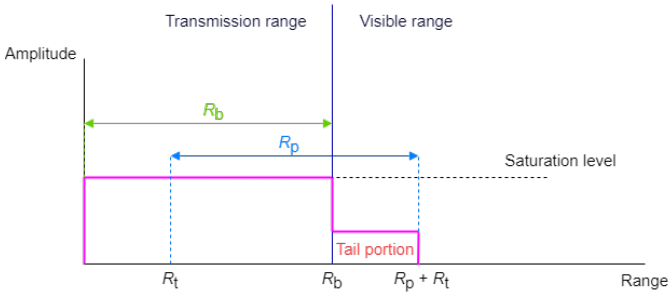


Fig. 6. Illustration of the uncontaminated tail portion of a target echo inside the transmission range. The tail portion is used for partial decoding in PPC. R_b is the transmission range. The received signal of the target echo located at R_t spans the range $R \in [R_t, R_t + R_p]$. Recall from Equation (1) that $R_p = R_b$.

The second step in the improved compression filter design is to apply an amplitude taper to the remaining non-zero samples of each improved compression filter using a window function. This step is designed to reduce the sidelobe levels causing the shoulder effect. The window function must be carefully tuned to reduce the sidelobe contamination and minimize the power loss in the compressed signal. An aggressive taper is more effective in mitigating the shoulders. However, it impacts the sensitivity of the system.

The aggressiveness of the taper can be changed based on the window function selected and its design parameters. In this article, a raised cosine (or Tukey) window function [24] is used. The roll-off factor used in the Tukey function (expressed as a normalized weight) is related to the number of samples modulated by the cosine. For example, if the roll-off factor is one, 100% of the elements are modulated (the most aggressive roll-off factor for the Tukey window). In contrast, if the roll-off factor is zero, the taper is equivalent to using a boxcar or rectangular window [24, 25]. An illustration of the window

(i.e., Tukey) used to produce the improved compression filter at the range R_t km (t_t μ s) is presented in Fig. 7.

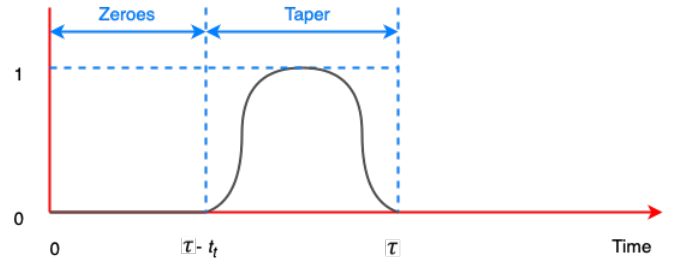


Fig. 7. Depiction of the window used to generate the improved compression filter at the range R_t km (t_t μ s).

The use of improved compression filters changes the modified pulse-compressed signal, previously derived in Salazar *et al.* [8],

$$y'(n) = \sum_{m=1}^M x'((m+n-1)T)x_f^*(m), \quad (2)$$

where, T is the radar sampling period, in units of s, $y'(n)$ is the value of the modified compressed signal at the range gate number n (nT in units of s, or $\frac{nTc}{2}$ in m), $x'(t_v)$ is the value of the modified received signal sampled at time t_v , (t_v in units of s), $x_f(m)$ is the value of the m^{th} sample on the compression filter, M is the number of samples in the compression filter (same number of samples as the transmitted signal), and $M \times T = \tau$. The new equation to calculate the compressed signal in PPC+ is

$$y'(n) = \sum_{m=1}^M x'((m+n-1)T)x_n^*(m), \quad (3)$$

where $x_n(m)$ is the value of the m^{th} sample in the improved compression filter designed for the range gate number n , defined as

$$x_n(m) = w_n(m)x_f(m), \quad (4)$$

where $w_n(m)$ is the value of the m^{th} sample in the window function to derive the improved compression filter $x_n(m)$. If the range gate number n is located outside the transmission range, the regular compression filter is used instead of the improved one, and then $x_n(m) = x_f(m)$.

In Equation (3), the complex conjugate of $x_n(m)$ is used,

$$x_n^*(m) = w_n^*(m)x_f^*(m). \quad (5)$$

Since the values in the $w_n(m)$ expression are not complex, then,

$$x_n^*(m) = w_n(m)x_f^*(m). \quad (6)$$

Additionally, it is necessary to recalculate the calibration factor used in PPC, to compensate for using the improved compression filters in PPC+. This is presented in the following section.

B. Calibration Factor

Salazar *et al.* [8] derived an equation to estimate the received compressed signal at the range gate number n ($y_e(n)$) as a function of $y'(n)$,

$$y_e(n) = s_+(n)y'(n), \quad (7)$$

where $s_+(n)$ is the value of new scaling factor calculated for the range gate number n . Then, combining (7) and (3) produces

$$y_e(n) = s_+(n) \sum_{m=1}^M x'((m+n-1)T)x_n^*(m). \quad (8)$$

The calibration or scaling factor $s_+(n)$ is derived from Equations (8) and the loss in SNR from a tapering equation presented by Bharadwaj and Chandrasekar [4], and it is approximately equal to

$$s_+(n) = s(n) \sqrt{\frac{M' \sum_{m'=1}^{M'} A(m')^2}{\left[\sum_{m'=1}^{M'} A(m') \right]^2}}. \quad (9)$$

where $s(n)$ is the calculation of the calibration factor for the range gate number n as it was derived for PPC [8], M' is the number of tapered samples on the improved compression filter, and $A(m')$ is the amplitude value of the m'^{th} tapered sample. The new calibration factor correctly estimates the fully compressed received signal inside the transmission range, including the effects of the improved compression filters. Nevertheless, using the improved compression filters affects the sensitivity of the radar inside the transmission range.

In the following section, the calculation of the radar sensitivity on radar systems using PPC+ is derived. Additionally, the radar sensitivity profile of PPC+ implemented on the PX-1000 radar is shown and compared to that of other blind-range mitigation techniques. The radar sensitivity is crucial on weather radars, and its analysis is an essential contribution of this work.

C. Sensitivity Analysis

The sensitivity function (Z_{\min}) is calculated using Equation (10) [8, 11, 26],

$$Z_{\min} \approx \frac{P_n 2^{10} \ln(2) \lambda^2 R^2 l^2 l_r}{\pi^3 P_t G^2 g_s \theta^2 c \tau |K_w|^2} \quad (10)$$

where P_n is the power from the noise floor, in W, λ is the wavelength of the radar, in m, R is the range, in m, l is the one-way attenuation or loss in the medium, unitless, l_r is a one-way loss factor due to the finite bandwidth of the receiver, unitless, P_t is the peak power that the radar transmits, in W, G is the antenna gain, unitless, g_s is the system power gain, unitless, θ is the 3-dB width of the one-way pattern, in radians, and K_w is the complex dielectric factor, unitless. K_w changes depending on the presence of water or ice. $|K_w|^2$ of ice is ≈ 0.18 , $|K_w|^2$ of water is ≈ 0.92 .

In PPC+, the improved compression filters affect the sensitivity of the radar system, generating a small loss compared to the original PPC. The sensitivity loss can be quantified

using the loss in SNR from a tapering equation presented by Bharadwaj and Chandrasekar [4],

$$L_w(n) = \frac{\left[\sum_{m=1}^M w(n+m-1)w_n(m) \right]^2}{M \left\{ \sum_{m=1}^M [w(n+m-1)w_n(m)]^2 \right\}}, \quad (11)$$

where $w(m)$ is the value of the m^{th} sample in the window function designed to mitigate the contamination resulting in the blind range, as described by Salazar *et al.* [8]. Then, for PPC+, the sensitivity (Z_{\min}) is approximately equal to

$$Z_{\min}(n) \approx \frac{P_n 2^{10} \ln(2) \lambda^2 R^2 l^2 l_r}{\pi^3 P_t L_w(n) G^2 g_s \theta^2 c \tau |K_w|^2}. \quad (12)$$

A comparison of the sensitivity profiles of PPC+, PPC, and the time-frequency multiplexing (TFM) method [5] is presented in Fig. 8, the lower the sensitivity value, the better it is. The TFM method transmits a short fill pulse multiplexed in time with the long pulse to mitigate the blind range. This technique was the default blind range mitigation solution for the PX-1000 system before implementing PPC.

Sensitivity profiles in Fig. 8 were calculated using a 67 μs optimized frequency modulated (OFM) waveform [7, 27]. Additionally, the improved compression filters used for PPC+ is designed with a Tukey window and a roll-off factor of one.

As seen in Fig. 8, implementing PPC+ impacts the sensitivity of the system when compared to the original PPC. Inside the transmission range, the sensitivity profile of PPC+ (green line) is approximately 2 to 3 dB higher than PPC (red line). This loss is observed throughout the transmission range and causes a small discontinuity in the PPC+ technique inside the transmission range. Nevertheless, even with the extra sensitivity loss inside the transmission range, PPC+ still provides better sensitivity than TFM (yellow line).

The use of PPC+ represents an improvement over the original PPC. The main advantages are the reduction in the mainlobe peak migration and the mitigation of the shoulder effect. Nevertheless, the PPC+ technique has some limitations to be discussed. One of the limitations is the decrease in the sensitivity inside the transmission range compared to PPC. An in-depth review of the advantages and limitations of PPC+ compared to PPC is presented in the following section.

D. Advantages and Limitations of PPC+

1) *Advantages of PPC+*: As explained in previous sections, the main improvements of PPC+ over PPC are the reduction in the mainlobe peak migration and the mitigation of the shoulder effect. These improvements can be inspected further by calculating the range-weighting function with PPC+ (the improved compression filters are designed using a Tukey window and roll-off factor of one), and a 67 μs OFM waveform. Improvements are illustrated in Fig. 9.

The range-weighting functions in Fig. 9 have been calculated for the same range gates as the ones presented in Fig. 4, as in Salazar *et al.* [8]. In Fig. 9, the shoulders observed when using PPC+ are less pronounced (narrower mainlobe) than those in PPC, especially in the range gates closer to the radar. Additionally, a significant reduction in the

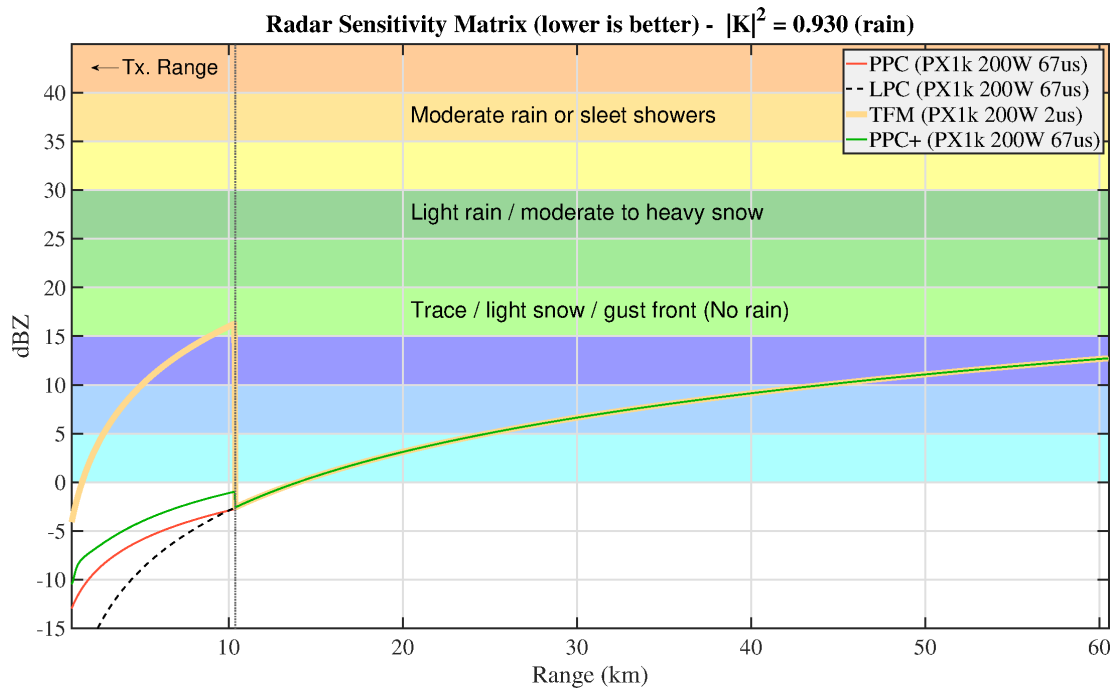


Fig. 8. Sensitivity profiles for different blind mitigation techniques implemented on PX-1000. The hypothetical sensitivity profile of the OFM waveform is included in the plot (black dashed line). Using the improved compression filters reduces the sensitivity of PPC+ compared to PPC inside the transmission range (Tx. range). Nonetheless, using PPC+ still provides significantly better sensitivity than TFM.

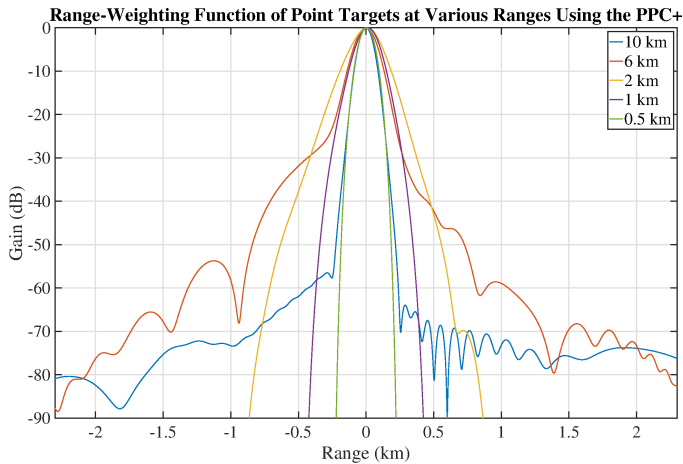


Fig. 9. Range-weighting function using PPC+ and based on the OFM waveform at different range gates. Comparing the results from PPC+ to the ones from PPC (see Fig. 4), it can be seen that the mainlobe peak migration is lower in PPC+, and the shoulder effect is less prominent. The shoulder reduction is more pronounced at closer ranges.

mainlobe peak migration is observed on PPC+ compared to PPC. Nevertheless, to better illustrate these improvements, the range-weighting functions at two range gates (1 and 8 km) are calculated with both PPC and PPC+ (see Fig. 10).

From Fig. 10, the shoulders in both range-weighting functions are lower when processed with PPC+. For the range gate at 1 km, sidelobes are at least 60 dB below the mainlobe, and no shoulders are visible on the plot. Concerning the mainlobe peak offset, a reduction is expected when using PPC+. Nevertheless, a zoomed-in version is shown in Fig. 11

to highlight this improvement. From Fig. 11, the mainlobe peak offset is visible on the range-weighting function from the range gate at 1 km using PPC. After implementing PPC+, the offset is still present but has been significantly reduced, from 30 m (when using PPC) to roughly 13 m.

Applying the improved compression filters on receive provides a simple and effective solution for the limitations observed in PPC. However, using PPC+ introduces some other limitations caused mainly by the amplitude taper used in the improved compression filters. These limitations will be discussed in the following section.

2) *Limitations of PPC+*: One of the limitations of PPC+ is that the radar sensitivity inside the transmission range is lower than that of PPC. The reduction is proportional to the difference in SNR gain between the improved compression filters and regular compression filter. Additionally, when using PPC+, there is a discontinuity at the end of the transmission range. This discontinuity is also proportional to the difference in SNR gain described before, but generally, it is much less significant than the one observed when using TFM (see Section II-C).

Additionally, using the improved compression filters widens the mainlobe width, affecting the range resolution of the compressed return. The reduction in range resolution is a by-product of using a window function and varies depending on the distance from the returned signal to the radar inside the transmission range. This effect is illustrated in Fig. 12.

In the top panel of Fig. 12, the range resolution resulting from the PPC+ processing (the improved compression filters are designed using a Tukey window and roll-off factor of one) is estimated as a function of range (based on the OFM

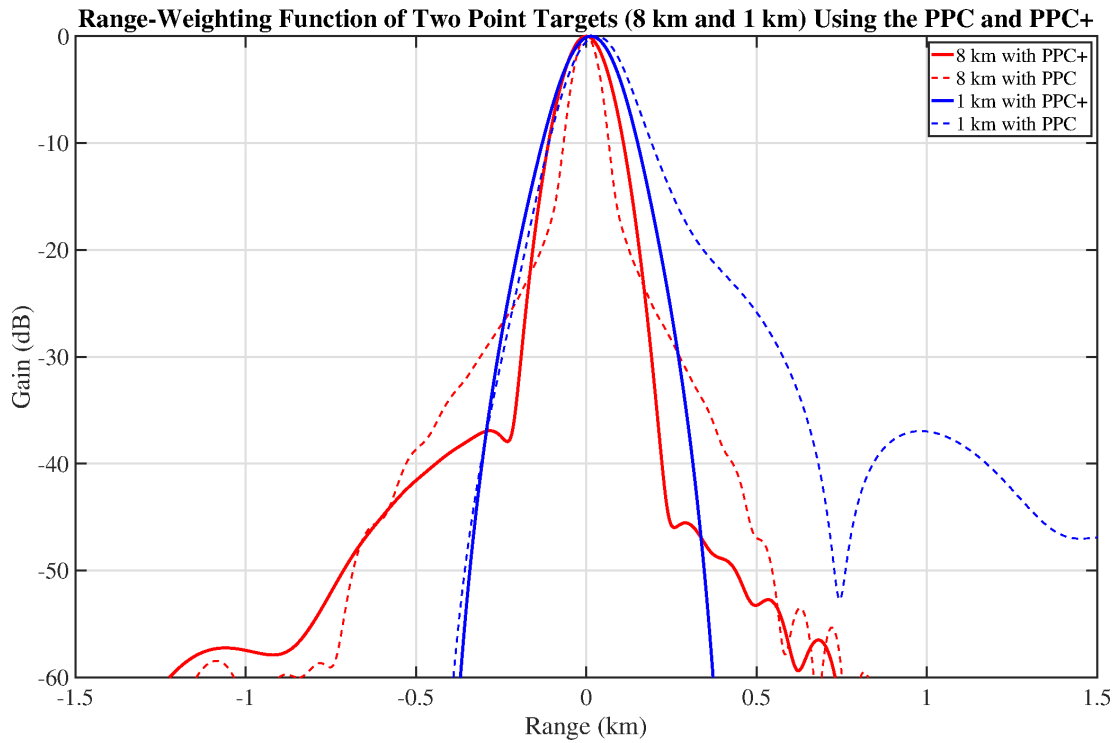


Fig. 10. Range-weighting functions for two range gates located 1 and 8 km from the radar (blue and red lines), using PPC (dashed lines) and PPC+ (solid lines). A noticeable reduction in the shoulder effect and mainlobe peak migration is observed in the PPC+ range-weighting functions.

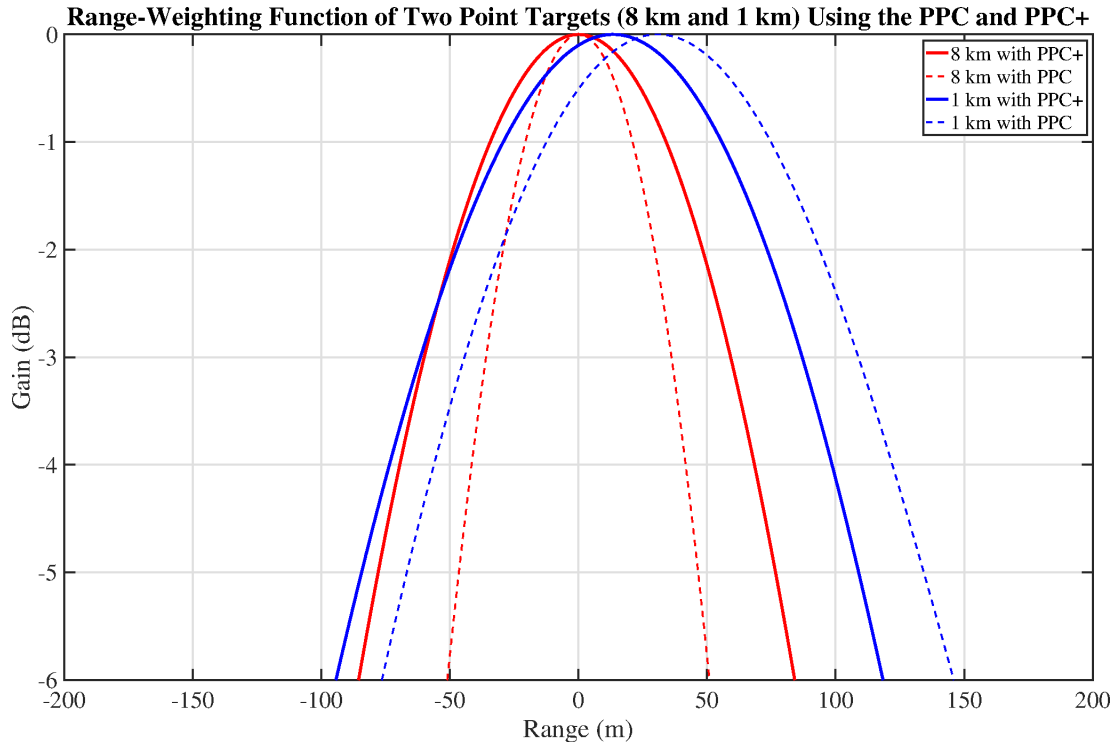


Fig. 11. Similar to Fig. 10, but zoomed in to observe the mainlobe peak locations.

waveform). The estimated range resolution is compared with the corresponding one using PPC. Also, a similar comparison is performed based on the estimated mainlobe peak offset as a function of range (see the bottom panel in Fig. 12).

From the top panel in Fig. 12, it is observed that using

improved compression filters in PPC+ negatively impacts the range resolution (lower than the one from PPC). The lower range resolution is observed in most range gates except those closest to the radar. In the closer range gates, the shoulders observed when using PPC are more prominent (broader and

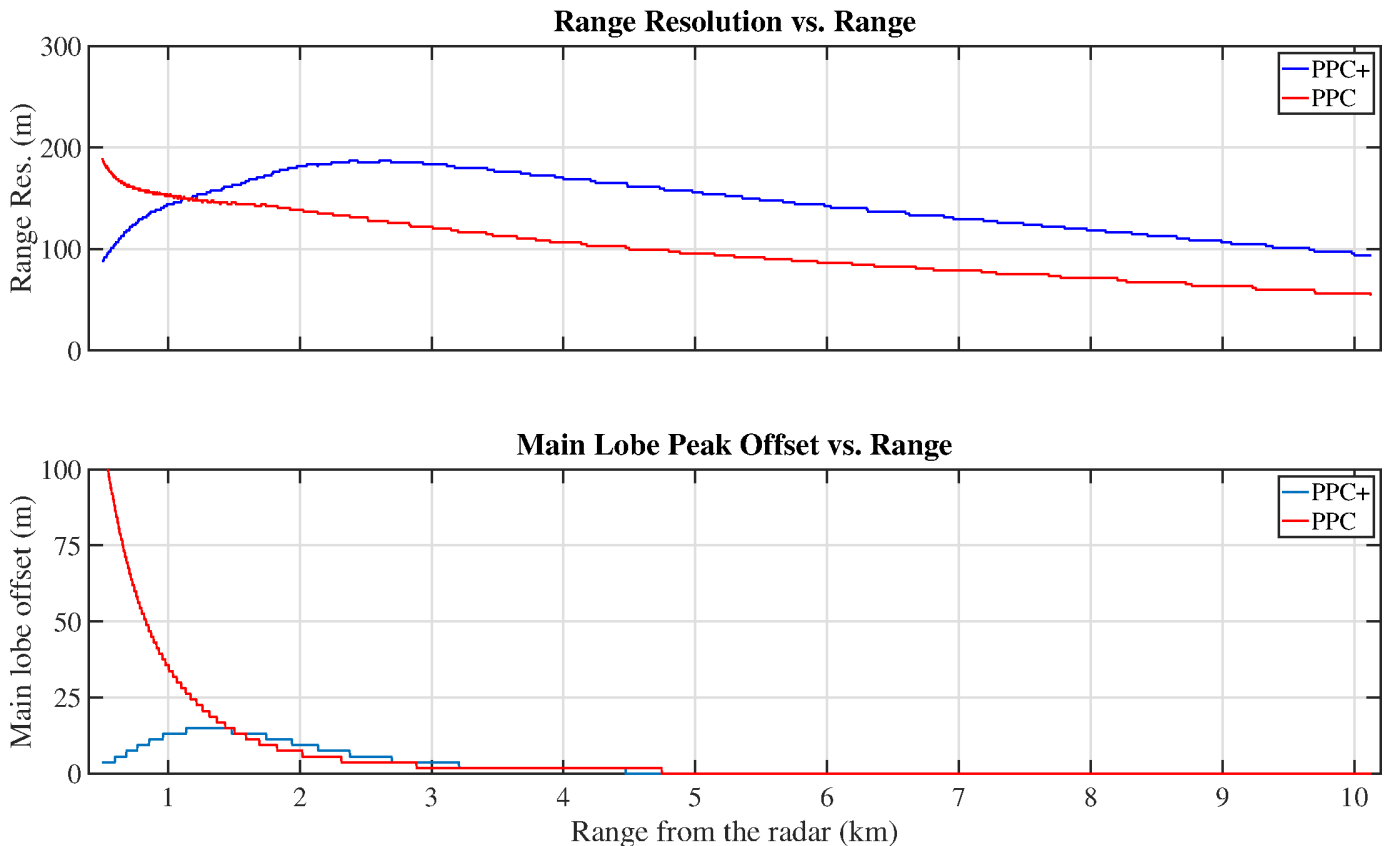


Fig. 12. A comparison of PPC and PPC+ concerning their performance in range solution and mainlobe peak offset inside the transmission range. The top and bottom panels show the range resolution and mainlobe peak offset as a range function. Results from PPC+ are compared with similar ones processed using PPC.

higher in magnitude), heavily affecting the range resolution. PPC+ mitigates the shoulders, improving the range resolution at these range gates. One could argue that the shoulder mitigation from PPC+ overcomes the loss in range resolution from the taper. Finally, in the lower panel of Fig. 12, it is observed that the mainlobe peak offset is significantly reduced when using PPC+. Nevertheless, even using the improved compression filters, the peak offset is not completely mitigated.

The limitations above are not related to using the improved compression filters but to using amplitude modulation in its design. It is theorized that using a set of compression filters modulated in amplitude and phase (rather than only in amplitude) might produce comparable shoulder mitigation and none of the limitations described before. Nevertheless, implementing compression filters using phase modulation is out of the scope of this work. Its design, analyses, and testing are proposed as a future research path to further improve PPC+.

III. RESULTS

In this section, PPC+ is evaluated using both simulated and real data collected from the PX-1000 radar system.

A. Simulations

A realistic simulation was performed to evaluate the performance of PPC+ and compare it to the original PPC. The

simulation is based on the work by Salazar *et al.* [8]. Aside from replacing PPC with PPC+ (the improved compression filters are designed using a Tukey window and roll-off factor of one), everything else remains the same. There are four point targets in the simulation, all simulated with an identical peak power. Two are located inside the transmission range while the other two are outside. The simulation was performed using the same $67 \mu\text{s}$ OFM pulse, and the exact location and peak power on the simulated point targets as those in Salazar *et al.* [8]. The simulation results are presented in Fig. 13.

In Fig. 13, the simulation setup and power profile from the PPC and PPC+ techniques are shown. The point targets locations are illustrated in the top panel, while the middle and bottom panels correspond to the results processed with PPC and PPC+. Both PPC and PPC+ correctly uncover the targets inside the blind range with an accurate estimation of their peak power. Moreover, as expected, PPC+ has less shoulder contamination than PPC. Nevertheless, shoulder contamination is not fully mitigated even when using PPC+. This behavior is more evident in the point targets located closer to the radar. In addition, the increase in the mainlobe width is noticeable on both point targets inside the transmission range (a trade-off that must be considered when designing the improved compression filters).

Concerning the mitigation of the mainlobe peak migration, it is unnoticeable in the example provided. As explained in

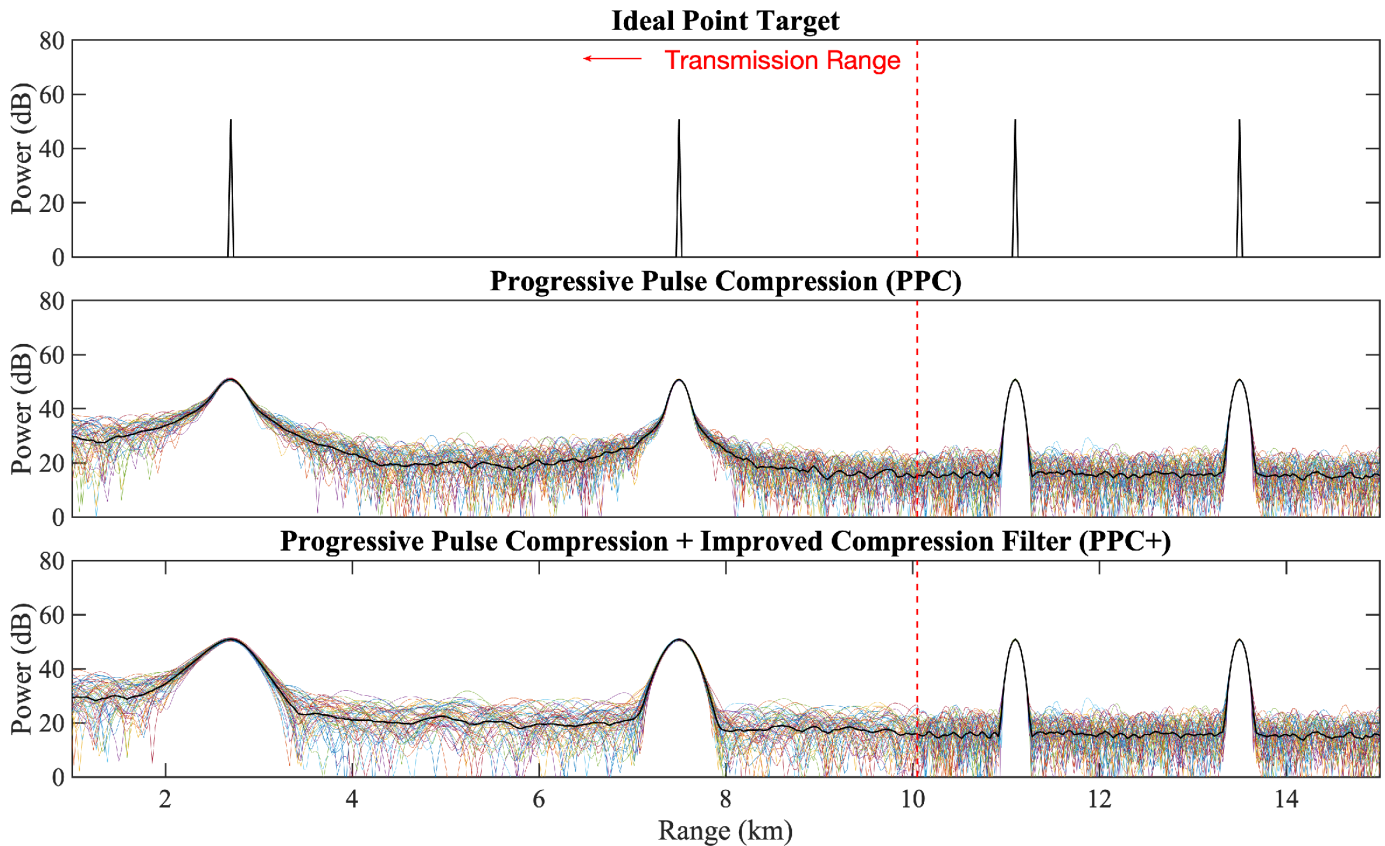


Fig. 13. Simulation results when transmitting the OFM waveform. The top plot illustrates the ideal location and power of the simulated point targets. In the middle panel, the simulation results from PPC are presented. Similar results are shown on the lower plot but from PPC+. Results using PPC+ have significantly reduced shoulder contamination compared to PPC.

the previous section, this effect is significant on point targets observed in the first one or two kilometers from the radar (see Fig. 12). Still, both point targets in this simulation are located in ranges where that effect is negligible.

B. Real Data

In this section, uncompressed polarimetric IQ data collected with the PX-1000 are processed using PPC and PPC+ (the improved compression filters are designed using a Tukey window and roll-off factor of one), and their performance inside the transmission range is compared. The radar was configured to transmit a $95 \mu\text{s}$ OFM pulse. Therefore, the transmission range is approximately 15 km. The dataset corresponds to a PPI scan collected during a winter storm in the Oklahoma City metropolitan area on January 30, 2023, 17:36 UTC, and with the radar scanning at an elevation of 4° .

The Z_h , radial velocity (v_r), Z_{DR} , and ρ_{hv} polarimetric variables are calculated from the IQ data and presented in Fig. 14. From panels (a), (c), (e), and (g) on Fig. 14, on the PPC column, there is a smeared weather returns (from green to blue on Z_h , fading towards the radar) located just west of the radar. This is an example of the shoulder contamination. The contamination can be observed in all polarimetric variables as a ray of similar values extending in range. PPC+ is capable of fully mitigating the shoulder, as seen in panels (b), (d), (f), and (h) on Fig. 14. When using PPC+, the edges of the storm

correspond more naturally to the expected values, and weaker returns are uncovered. For example, comparing the ρ_{hv} panels on the closer edge of the storm located west, it is observed that, when processed using PPC+, the correlation coefficient is roughly 94%. Nevertheless, when processed using PPC, this edge was covered and showed different correlation values.

The shoulder effect can be subtle enough to be misrepresented as part of the weather when it is located within it. This is observed in the portion of the storm located northwest of the radar. When the IQ data are processed with PPC, the edge of the storm, located close to and inside the transmission range, does not exhibit evidence of shoulders. Nevertheless, some hints suggesting contamination can be observed in the v_r and ρ_{hv} plots. In both panels, slight smearing is observable, but the same is hardly noticeable in the other panels. When processing using PPC+, and the same area is inspected, no smearing is present, and the values of the polarimetric variables are different. The previous confirms that the shoulders were contaminating that area and proves how effective PPC+ is in mitigating them.

To illustrate the shoulder contamination mitigated by using PPC+, the Z_h values from the original PPC (panel (a) in Fig. 14) and PPC+ (panel (b) in Fig. 14) were subtracted. The previous calculation overlaps with the contour of the weather observable when using PPC+ (panel (b) in Fig. 14) and is presented in Fig. 15.

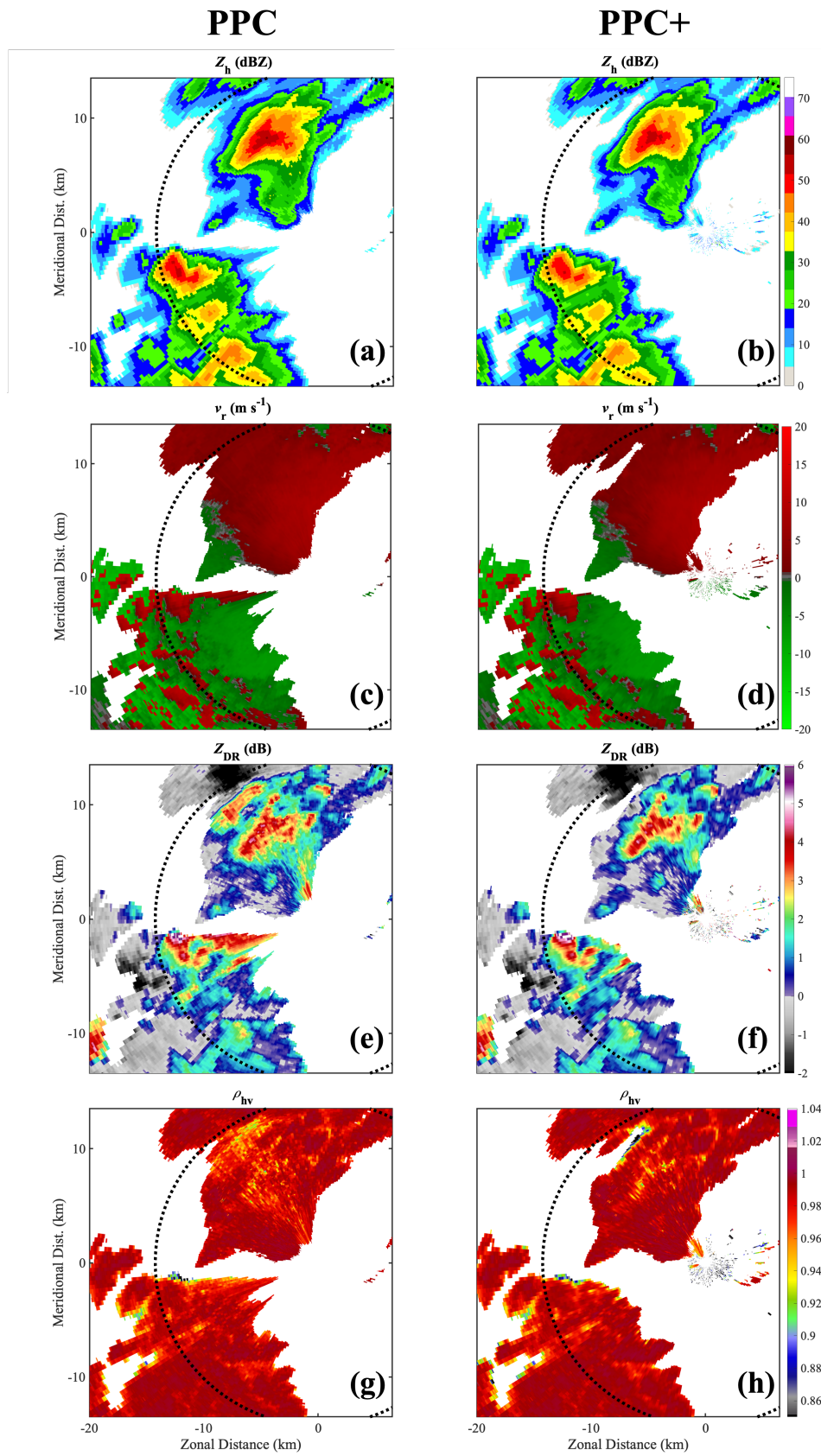


Fig. 14. PPIs of different radar variables processed with PPC and PPC+ from a winter storm in the Oklahoma City metropolitan area on January 30, 2023, 17:36 UTC, at an elevation of 4° . Polarimetric variables processed using PPC: (a) Z_h , (c) v_r , (e) Z_{DR} , (g) ρ_{hv} . Polarimetric variables processed using PPC+: (b) Z_h , (d) v_r , (f) Z_{DR} , (h) ρ_{hv} . In the PPC+ plots, it is shown that the shoulders, contaminating the echoes from PPC (inside the transmission range), have been greatly reduced.

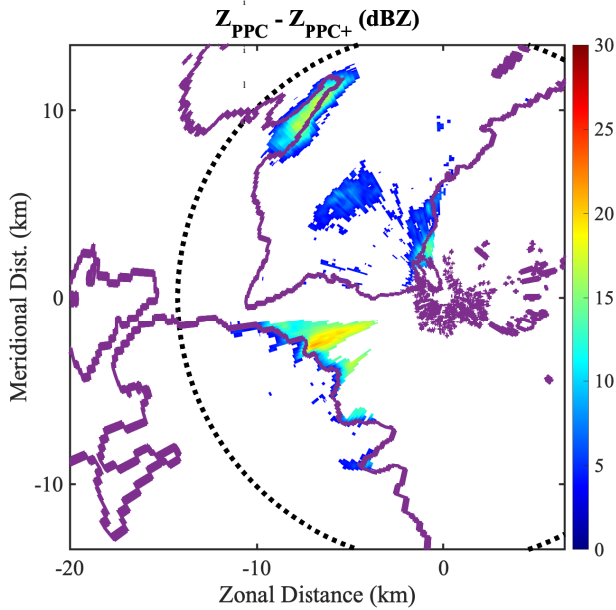


Fig. 15. Difference of the Z_h values from the original PPC (panel (a) in Fig. 14) and PPC+ (panel (b) in Fig. 14) overlapped with the contour of the weather observable when using PPC+ (panel (b) in Fig. 14).

In Fig. 15, a quantitative metric of the shoulder contamination and the regions where it was present are illustrated. Additionally, if the shoulders overpower and obscure any weather, it will be preserved when using PPC+, as noticeable by the overlap with the contour lines. Then, PPC+ can mitigate the limitations of PPC while maintaining its performance as a blind range mitigation technique.

IV. DISCUSSION AND CONCLUSIONS

The PPC technique described in Salazar *et al.* [8] has proven to be a significant improvement in mitigating the blind range problem. Nevertheless, the PPC users have pointed out some limitations on different datasets collected since its inception. The two most problematic limitations are the shoulder effect and the mainlobe peak migration. An improved version of PPC, named PPC+, has been proposed in this article. The PPC+ technique is capable of mitigating the limitations of PPC, producing high-quality polarimetric weather observations while maintaining its blind range mitigation capabilities, which is of critical importance for the radar meteorology community.

The PPC+ technique uses a set of improved compression filters, changing as a function of range, to compress the incomplete return. The improved compression filters can be designed using amplitude or phase modulation. In this research, the improved compression filters are designed by amplitude modulating (multiplying by a window function) the original filter. The first portion of the window will have as many zeroes as the corresponding incomplete return (at a specific range). Then, a taper in amplitude is applied to the remaining non-zero samples of the window function. The zeroed-out portion of the improved compression filters reduces the mainlobe peak shift and tapering the remaining portion

reduces the sidelobe levels causing the shoulder effect. The design of the improved compression filters is one important contribution of this work.

The PPC+ methodology is similar to the one from PPC. Nevertheless, there are some changes to be discussed. One is that the modified pulse-compressed signal is obtained by compressing the modified return signal with the improved compression filters. Consequently, it is necessary to design a new calibration factor for PPC+ to account for using the improved compression filters.

The improved calibration factor is critical for the weather radar community and is another essential contribution of this work. Correctly calibrating the compressed IQ data in PPC+ allows the estimation of the unaltered data from scatterers within the transmission range, facilitating accurate calculations of polarimetric variables and improving the polarimetric quality of the weather observations.

The PPC+ implementation discussed in this work has two main limitations: decreased range resolution and sensitivity inside the transmission range. However, even though these limitations negatively impact the performance of PPC+, it is still superior to other blind range mitigation techniques using fill pulses (e.g., George *et al.* [3], Bharadwaj and Chandrasekar [4], and Cheong *et al.* [5]).

The previously discussed limitations are not inherent to PPC+, but rather to using amplitude modulation to design the improved compression filters. It is theorized that using a combination of amplitude and phase modulation will result in similar mitigation of the shoulder effect and mainlobe peak migration but with a lower impact on sensitivity and range resolution. The use of phase modulation in the design of the improved compression filters is a topic for future research.

Simulation and experimental results show improvements in PPC+ compared to the original PPC. In the simulation, both point targets inside the transmission range have considerably lower shoulders when compressed using PPC+. Nevertheless, the decrease in the range resolution on those point targets can also be observed. Concerning the experimental results, there is observed that the shoulder effect is greatly mitigated. The loss in range resolution is still present, but it is not as noticeable as with point targets.

The PPC+ technique represents an essential improvement over PPC. Moreover, like the original PPC, no hardware modification is required to implement it, and it is compatible with any radar system using pulse compression. Furthermore, with a modest amount of effort, it can be implemented as a software update on systems using PPC. The PX-1000 is the first system where PPC+ is being used. PPC+ has been recently implemented as a software update on PX-1000, and data processed using it can be visualized through the RadarHub (<https://radarhub.rrc.ou.edu>), offering a variety of practical examples of the performance of PPC+ in different weather scenarios. It has also been implemented in Horus, an all-digital phased array radar recently completed at the ARRC [19–21]. The implementation of PPC+ in PX-1000 and Horus is a significant contribution since one of the takeouts of this work is that PPC+ can be easily implemented on any radar without any hardware modifications and with good

polarimetric quality, and now a good repository of data from PX-1000 is available online to support this affirmation.

V. ACKNOWLEDGMENTS

The authors would like to thank anonymous reviewers for comments that improved this manuscript. This work is supported by the NOAA/Office of Oceanic and Atmospheric Research under NOAA-University of Oklahoma Cooperative Agreement #NA21OAR4320204, U.S. Department of Commerce. Real-time and archived data from the PX-1000 can be visualized through the RadarHub (<https://radarhub.arcc.ou.edu>), and IQ data are available from the authors upon request.

REFERENCES

- [1] F. O’Hora and J. Bech, “Improving Weather Radar Observations Using Pulse-Compression Techniques,” *Meteorological Applications*, vol. 14, pp. 389–401, 2007. DOI: 10.1002/met.38.
- [2] J. George, N. Bharadwaj, and V. Chandrasekar, “Considerations in Pulse Compression Design for Weather Radars,” in *IGARSS 2008 - 2008 IEEE International Geoscience and Remote Sensing Symposium*, vol. 5, 2008, pp. V - 109-V -112. DOI: 10.1109/IGARSS.2008.4780039.
- [3] J. George, K. V. Mishra, C. M. Nguyen, and V. Chandrasekar, “Implementation of Blind Zone and Range-Velocity Ambiguity Mitigation for Solid-State Weather Radar,” in *2010 IEEE Radar Conference*, 2010, pp. 1434–1438. DOI: 10.1109/RADAR.2010.5494392.
- [4] N. Bharadwaj and V. Chandrasekar, “Wideband Waveform Design Principles for Solid-State Weather Radars,” *J. Atmos. Oceanic Technol.*, vol. 29(1), pp. 14–31, 2012. DOI: <https://doi.org/10.1175/JTECH-D-11-00030.1>.
- [5] B. L. Cheong, K. Redmond, R. D. Palmer, Y. Zhang, M. Yearly, and T.-Y. Yu, “PX-1000: A Solid-State Polarimetric X-Band Weather Radar and Time-Frequency Multiplexed Waveform for Blind Range Mitigation,” *IEEE Trans. Instrum. Meas.*, vol. 62(11), pp. 3064–3072, 2013. DOI: 0.1109/TIM.2013.2270046.
- [6] C. M. Nguyen and V. Chandrasekar, “Sensitivity Enhancement System for Pulse Compression Weather Radar,” *Journal of Atmospheric and Oceanic Technology*, vol. 31, no. 12, pp. 2732–2748, 2014. DOI: 10.1175/JTECH-D-14-00049.1.
- [7] J. M. Kurdzo, B. L. Cheong, R. D. Palmer, G. Zhang, and J. B. Meier, “A Pulse Compression Waveform for Improved-Sensitivity Weather Radar Observations,” *Journal of Atmospheric and Oceanic Technology*, vol. 31, no. 12, pp. 2713–2731, 2014. DOI: 10.1175/JTECH-D-13-00021.1.
- [8] C. Salazar, B. Cheong, and R. D. Palmer, “Progressive Pulse Compression: A Novel Technique for Blind Range Recovery for Solid-State Radars,” *Journal of Atmospheric and Oceanic Technology*, vol. 38, no. 9, pp. 1599–1611, 2021. DOI: 10.1175/JTECH-D-20-0164.1.
- [9] R. J. Keeler and C. A. Hwang, “Pulse Compression for Weather Radar,” in *Proceedings International Radar Conference*, 1995, pp. 529–535. DOI: 10.1109/RADAR.1995.522603.
- [10] S. M. Torres, C. D. Curtis, and D. Schwartzman, “Requirement-Driven Design of Pulse Compression Waveforms for Weather Radars,” *Journal of Atmospheric and Oceanic Technology*, vol. 34, no. 6, pp. 1351–1369, 2017. DOI: 10.1175/JTECH-D-16-0231.1.
- [11] C. Salazar, “Breaking the Practical Performance Barriers of Polarimetric Phased Array Weather Radars,” Ph.D. dissertation, The University of Oklahoma, Norman, OK, USA, 2022.
- [12] T. Mega, K. Monden, T. Ushio, K. Okamoto, Z.-I. Kawasaki, and T. Morimoto, “A Low-Power High-Resolution Broad-Band Radar Using a Pulse Compression Technique for Meteorological Application,” *IEEE Geoscience and Remote Sensing Letters*, vol. 4, no. 3, pp. 392–396, 2007.
- [13] E. Yoshikawa *et al.*, “Development and initial observation of high-resolution volume-scanning radar for meteorological application,” *IEEE Transactions on geoscience and remote sensing*, vol. 48, no. 8, pp. 3225–3235, 2010.
- [14] E. Yoshikawa, S. Kida, S. Yoshida, T. Morimoto, T. Ushio, and Z. Kawasaki, “Vertical Structure of Raindrop Size Distribution in Lower Atmospheric Boundary Layer,” *Geophysical research letters*, vol. 37, no. 20, 2010.
- [15] D. Lamper and T. L. Grettenberg, *Pulse Compression Technique for High Duty Factor Radar*, US Patent 5,036,324, Jul. 1991.
- [16] L. Pralon, B. Pompeo, G. Beltrao, H. Cioqueta, B. Cosenza, and J. Moreira, “On a Blind Zone Elimination Method Based on Partial Compression Filter Design Using Random Waveforms for Monostatic Pulsed Radars,” in *IET International Conference on Radar Systems (Radar 2012)*, 2012, pp. 1–5. DOI: 10.1049/cp.2012.1653.
- [17] V. M. Melnikov and D. S. Zrnić, “On the Alternate Transmission Mode for Polarimetric Phased Array Weather Radar,” *Journal of Atmospheric and Oceanic Technology*, vol. 32, no. 2, pp. 220–233, 2015. DOI: 10.1175/JTECH-D-13-00176.1.
- [18] A. Ryzhkov *et al.*, “Quasi-Vertical Profiles—A New Way to Look at Polarimetric Radar Data,” *Journal of Atmospheric and Oceanic Technology*, vol. 33, no. 3, pp. 551–562, 2016.
- [19] R. D. Palmer, C. J. Fulton, J. Salazar, H. Sigmarsson, and M. Yearly, “The ‘Horus’ Radar—an All-Digital Polarimetric Phased Array Radar for Multi-Mission Surveillance,” in *99th American Meteorological Society Annual Meeting*, AMS, 2019.
- [20] C. Fulton *et al.*, “Horus: A Testbed for Fully Digital Phased Array Radars,” *Microwave Journal*, vol. 63, no. 1, pp. 20–36, Jan. 2020.

- [21] R. D. Palmer *et al.*, “Horus – A Fully Digital Polarimetric Phased Array Radar for Next-Generation Weather Observations,” *IEEE Transactions on Radar Systems*, vol. 1, pp. 96–117, 2023. DOI: 10.1109/TRS.2023.3280033.
- [22] D. Schwartzman and S. Torres, “Design of Practical Pulse Compression Waveforms for Polarimetric Phased Array Radar,” in *Proc. 39th Int. Conf. Radar Meteorol.*, 2019, pp. 1–9.
- [23] C. Salazar, R. D. Palmer, and B. L. Cheong, “Methods and Apparatus for Blind Range Recovery on Pulse Compression Radars,” US Patent 11,313,959, Apr. 2022.
- [24] J. Kaimal and L. Kristensen, “Time Series Tapering for Short Data Samples,” *Boundary-layer meteorology*, vol. 57, no. 1, pp. 187–194, 1991.
- [25] P. Bloomfield, *Fourier Analysis of Time Series: an Introduction*. John Wiley & Sons, 2004.
- [26] R. J. Doviak and D. Zrnic, *Doppler Radar and Weather Observations*. Dover Publications, Inc., 1993.
- [27] J. Kurdzo, “Pulse Compression Waveforms and Applications for Weather Radar,” Available at <https://shareok.org/handle/11244/23250>, Ph.D. dissertation, The University of Oklahoma, Norman, OK, USA, 2015.



Cesar M. Salazar (S'21-M'23) was born in Chiclayo, Lambayeque, Peru, on March 16, 1992. He received a B.S. degree in industrial engineering from the University of San Martin de Porres, Peru, in 2012, an M.S. degree in industrial engineering from the University of Puerto Rico at Mayaguez, Mayaguez, Puerto Rico, USA, in 2017, and a Ph.D. degree in electrical and computer engineering from The University of Oklahoma (O.U.), Norman, OK, USA, in 2022. During his Ph.D., he was a graduate research assistant with the Advanced Radar Research Center (ARRC) at OU. After graduating, he worked as a Postdoctoral fellow for the ARRC from December 2022 to May 2023. He is a postdoctoral fellow with the Cooperative Institute for Severe and High-Impact Weather Research and Operations (CIWRO) at OU.

His research interests include developing novel signal processing solutions to alleviate the most critical limitations observed in polarimetric weather phased array radars. He is especially interested in cost-efficient solutions that are easy to implement and require no hardware modifications on the intended systems. Additionally, he is interested in estimating atmospheric variables using statistical analysis, remote sensing, and signal processing. He is especially interested in developing algorithms to estimate atmospheric variables with high temporal and spatial resolution.



Boonleng Cheong received his Ph.D. degree in electrical engineering from the University of Nebraska–Lincoln, Lincoln, Nebraska, in 2005, with a dissertation titled Adaptive Beamforming to Observe the Atmospheric Boundary Layer Using the Turbulent Eddy Profiler. He joined the University of Oklahoma (OU) immediately after his graduation. From 2005–2007, he was a postdoctoral fellow with the School of Meteorology. The opportunity allowed him to utilize his expertise in digital signal processing in the areas of remote sensing using ground-based radars. Since 2008, he joined the Advanced Radar Research Center (ARRC) as a research scientist. He also currently affiliated with the School of Electrical and Computer Engineering (ECE) as an Adjunct Associate Professor and the Cooperative Institute for Severe and High-Impact Weather Research and Operations (CIWRO) as an executive board member and fellow.

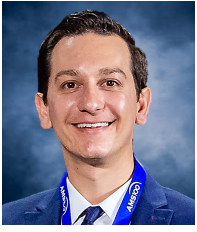
His research interests include modern software-defined radar design, array signal processing, real-time software architecture, parallel computing, numerical simulations and artificial intelligence using deep learning. He is the key developer of the PX-1000 and PX-10k systems, which are solid-state based X-band polarimetric transportable radars. Throughout his career, he has published in several internationally recognized scholarly journal magazines. He has authored and co-authored more than 40 peer-reviewed journal articles and over 100 conference presentations and invited talks.



Robert D. Palmer (Fellow, IEEE) was born in Fort Benning, GA on June 3, 1962. He received the Ph.D. degree in electrical engineering from the University of Oklahoma, Norman, OK, USA, in 1989.

From 1989 to 1991, he was a JSPS Post-Doctoral Fellow with the Radio Atmospheric Science Center, Kyoto University, Japan, where his major accomplishment was the development of novel interferometric radar techniques for studies of atmospheric turbulent layers. After his stay in Japan, he was with the Department of Physics and Astronomy, Clemson University, South Carolina. From 1993 to 2004, he was a part of the faculty of the Department of Electrical Engineering, University of Nebraska–Lincoln, where his interests broadened into areas including wireless communications, remote sensing, and pedagogy. Soon after moving to OU as the Tommy C. Craighead Chair at the School of Meteorology in 2004, he established the interdisciplinary Advanced Radar Research Center (ARRC). He currently serves as the Executive Director for the ARRC and OU’s Associate Vice President for Research and Partnerships. While at OU, his research interests have focused on the application of advanced radar signal processing techniques to observations of severe weather, particularly related to phased-array radars and other innovative system designs. He has published widely in the area of radar sensing of the atmosphere, with over 115 peer-reviewed journal articles, one textbook, 40 international invited talks, and more than 300 conference presentations.

Prof. Palmer is also a fellow of the American Meteorological Society (AMS) emphasizing his dedication to the interdisciplinary nature of radar science.



David Schwartzman (S'09-M'20-SM'22) was born in Piracicaba, SP, Brazil, on March 17, 1988. He received the B.S. degree in electrical and computer engineering from the National University of Asunción, San Lorenzo, Paraguay, in 2011, and the M.S. and Ph.D. degrees in electrical and computer engineering from the University of Oklahoma, Norman, OK, USA, in 2015 and 2020, respectively. From 2015 to 2020, he was a Research Scientist with the NOAA National Severe Storms Laboratory (NSSL) and the Cooperative Institute for Severe and High-Impact

Weather Research and Operations (CIWRO). From 2021 to mid-2022, he was a Research Scientist with the Advanced Radar Research Center (ARRC) at The University of Oklahoma. Currently, he is an Assistant Professor with the University of Oklahoma School of Meteorology, affiliated with the ARRC. He works on novel signal and array processing algorithms to improve understanding of atmospheric processes using phased array radar. He also works on calibration and integration of phased array radar systems.

Dr. Schwartzman is also an Adjunct Assistant Professor with the University of Oklahoma School of Electrical and Computer Engineering. He is the recipient of the 2022 IEEE R5 *Outstanding Young Professional* Award and the 2019 American Meteorological Society's *Spiros G. Geotis* Prize. He is a Senior Member of the Institute for Electrical and Electronic Engineers (IEEE) and a member of the American Meteorological Society (AMS).



Alexander V. Ryzhkov received the M.S. and Ph.D. degrees in radio science from Leningrad State University, St. Petersburg, Russia, in 1974 and 1977, respectively. From 1978 to 1992, he was with the Main Geophysical Observatory, Leningrad, Russia. In 1992, he joined the National Severe Storms Laboratory, Norman, OK, USA, and the Cooperative Institute for Mesoscale Meteorological Studies, University of Oklahoma, Norman, where he has been a Senior Research Scientist since 1995. In 2021 the Institute became Cooperative Institute for Severe and

High-Impact Weather Research and Operations. He contributed extensively to the development of polarimetric radar algorithms for quantitative precipitation estimation, hydrometeor classification, and microphysical retrievals and their operational applications on the U.S. National Weather Service WSR-88D weather radar network. His current research interests include atmospheric remote sensing, radiowave propagation, cloud microphysics, and radar meteorology with a focus on Doppler polarimetric radars.